ELSEVIER

Chemosphere 64 (2006) 1920–1928

CHEMOSPHERE

www.elsevier.com/locate/chemosphere

Adsorption of basic dyes onto MCM-41

Lain-Chuen Juang *, Cheng-Cai Wang, Chung-Kung Lee

Green Environment R&D Center and Department of Environmental Engineering, Vanung University, Chung-Li, 320 Taiwan, ROC

Received 26 June 2005; received in revised form 9 January 2006; accepted 10 January 2006
Available online 17 February 2006

Abstract

The adsorption of two basic dyes, Basic Green 5 (BG5) and Basic Violet 10 (BV10), onto MCM-41 was studied to examine the possible effect of interactions between large adsorbates and MCM-41 on the pore structure stability of MCM-41 and the potential of MCM-41 for the removal of basic dyes from wastewater. The revolutions of surface characteristics and pore structure of MCM-41 induced by dyes adsorption were characterized based on the analyses of the nitrogen isotherms, the XRD patterns, and the FTIR spectra. It was experimentally concluded that when the effect of interactions between large dyes (such as BV10) and MCM-41 on the pore structure stability of MCM-41 was insignificant, MCM-41 might be a good adsorbent for the removal of basic dyes from wastewater. The adsorption of BV10 on MCM-41 with respect to contact time, pH, and temperature was then measured to provide more information about the adsorption characteristics of MCM-41. Both Langmuir and Freundlich adsorption models were applied to describe the equilibrium isotherms and the pseudo-second-order kinetic model was used to describe the kinetic data, from which some adsorption thermodynamic parameters were also evaluated.

Keywords: MCM-41; Basic dyes; Adsorption; Pore structure stability; Interaction

1. Introduction

The discovery of ordered mesoporous materials has led to the explosive growth of research in the synthesis, characterization, and application of these materials (Zhao et al., 1996; Corma, 1997; Ying et al., 1999; Selvam et al., 2001). As one of these materials, MCM-41 provides exciting opportunities for fundamental and applied studies on mesoporous materials. Such material is characterized by high surface area, high pore volume, as well as parallel and ideally shaped pore structures without the complications of a network. The cylindrical pore structure and high degree of pore symmetry found in ordered mesoporous silica are ideal for testing various existing adsorption and diffusion models (Storck et al., 1998; Choma et al., 2001; Ribeiro Carrott et al., 2001; Wloch et al., 2002). Moreover, its unique pore structures also offer a special environment for chemical separations (Thomas, 1994) and reactions (Corma, 1997). On the other hand, chemical modifications of MCM-41 are successful in tailoring the physical, chemical, and catalytic properties of these materials, which in turn increases their applications (Aronson et al., 1997; Zhao et al., 2000).

In the literature, the studies on the adsorption and transport of MCM-41 were concentrated on gases (Hansen et al., 1998; Choudhary and Mantri, 2000; Hu et al., 2001; Zhao et al., 2001; Oh et al., 2003; Lee et al., 2004) with very few investigations dealing with the liquid-phase system (Liu et al., 1998; Nooney et al., 2001 Ghiaci et al., 2004). However, MCM-41 may also have potential for liquid-phase separations and reactions. Among them, some applications involving liquid-phase systems have demonstrated the capability of MCM-41 in dealing with pollution problems, such as the removal of mercury and other heavy metals from water (Liu et al., 1998). Recently, Ho et al.

* Corresponding author. Tel.: +886 3 4342379x64; fax: +886 3 4622232.
E-mail addresses: lcjuang@msa.vnu.edu.tw (L.-C. Juang), anthony@msa.vnu.edu.tw (C.-K. Lee).

0045-6535/$ - see front matter © 2006 Elsevier Ltd. All rights reserved.
doi:10.1016/j.chemosphere.2006.01.024

(2003) have shown that materials prepared by grafting amino- and carboxylic-containing functional groups onto MCM-41 might be a useful adsorbent for the removal of Acid blue 25 and Methylene blue dyes from wastewater and these adsorbents can be regenerated by simple washing with alkaline or acid solution to recover the adsorbents and adsorbed dyes. For these adsorption investigations, it was found that the interactions between adsorbates and surface functional groups of MCM-41 might play a key role on the determination of adsorption properties of the original and chemical modified MCM-41 samples. Because one main obstacle for the widespread industrial application of ordered mesoporous silica is its structure stability, the effects of interaction between large adsorbates (e.g., dyes) and adsorbents on the pore structure stability of MCM-41 must first be examined.

In the present study, our objective is to examine the possible effect of interactions between large dyes and MCM-41 on the pore structure of MCM-41 and the potential of MCM-41 for the removal of dyes from wastewater by measuring the adsorption data of two basic dyes, BG5 and BV10. The changes of surface characteristics and pore structure of MCM-41 introduced by dyes adsorption were characterized based on the analyses of the nitrogen adsorption isotherms, the XRD patterns, and the FTIR spectra. The relationship between the alteration in the pore structure and the change in the adsorption capacity of MCM-41 was discussed. Moreover, for dye with high adsorption capacity, the adsorption processes with respect to pH, contact time, and temperature was also measured to provide more information about the adsorption characteristics of MCM-41. The equilibrium data were fitted into Langmuir and Freundlich equations to determine the correlation between the isotherm models and experimental data. The kinetic and thermodynamic parameters were calculated to determine the adsorption mechanism.

2. Materials and adsorption isotherms

2.1. Adsorbent

Mesoporous MCM-41 has been successfully prepared using different synthesis procedures and conditions (Ying et al., 1999). For this study, the MCM-41 powder was crystallized from an alkaline solution containing cetyltrimethylammonium bromide (CTABr, 99%, Merck), sodium silicate solution (Na_2O, 7.5–8.5%, SiO_2, 25.8–28.5%, Merck), sulfuric acid (98%, Merck), and deionized water in the mole ratio of 1 CTABr:1.76 Na_2O:6.14 SiO_2:335.23 H_2O:1.07 H_2SO_4. After 24 h of crystallization at room temperature, the MCM-41 powder was filtered, washed, and dried before it was calcined in a furnace at 450 °C for 4 h to remove the organic template. The particle size distribution of the obtained MCM-41 measured with the zeta potential analyzer (Nano ZS, Malvern) was concentrated at 50–60 nm.

2.2. Adsorbates

BG5 and BV10 were selected as adsorbates to discuss the adsorption selectivity of MCM-41 in terms of pore structure of adsorbent and molecular shape of adsorbates. Both compounds were of analytical grade from Sigma Chemical Co. (USA) and were used without further purification. The structures of both dyes are shown in Fig. 1.

2.3. Adsorption measurements

The dye adsorption data from water solutions were obtained by the immersion method. BG5 and BV10 were first dried at 105 °C for 24 h to remove moisture before use. All of the dye solution was prepared with distilled water. For adsorption experiments, 0.1-g-MCM-41 was added into 100 ml of dye water solutions at the desired concentration. The pH of the solution was adjusted with NaOH or HCl solution to maintain a constant value. The preliminary experiment revealed that about 50 min was required for the adsorption process to reach equilibrium with a reciprocating shaker. The solution and solid phase were separated by centrifugation at 8000 rpm for 25 min in a Sorvall RC-5C centrifuge. A 15-ml aliquot of the supernatant was removed and analyzed for BG5 and BV10 by UV (Hitachi, U-2000) at the wave length of 655 and 555 nm, respectively. The adsorption capacity of dyes was then calculated using the relation $Q = V\Delta C/m$, where V was the volume of the liquid phase, m was the mass of the solid, and ΔC was the difference between the initial and final concentration of dye at solutions, which could be computed simply from the initial and final UV readings. For the experiments of adsorption kinetics, the dye

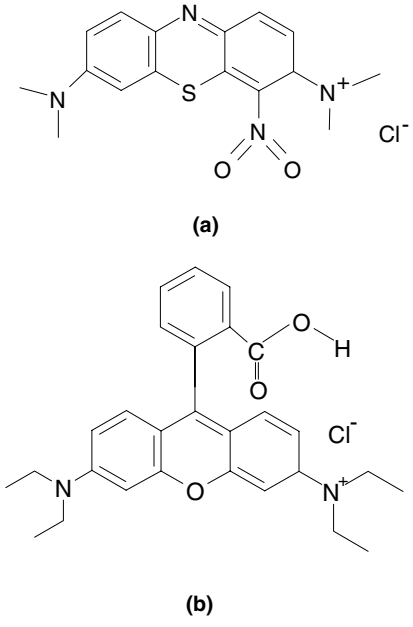

Fig. 1. The structures of basic dyes: (a) BG5 and (b) BV10.

adsorption amounts were determined by analyzing the solution at appropriate time intervals.

The effects of temperature and pH on the adsorption data were carried out by performing the adsorption experiments at various temperatures (25, 45, and 65 °C) and various pHs (2–11), respectively.

The phase structure and pore size of the MCM-41 samples before and after adsorbing dye were evaluated from the X-ray diffraction patterns obtained from Thermal ARL X-ray diffractometer equipped with a Cu Kα radiation source and a graphite monochromator. The porous structure characteristics including surface area and pore volume were obtained from the conventional analysis of nitrogen isotherms measured at 77 K with Micromeritics TriStar 3000 apparatus. Fourier transform infrared (FTIR) spectra of MCM-41 samples were recorded using a Perkin Elemer Model 1600 FTIR spectrophotometer over the range 4000–400 cm^{-1}. IR spectra were obtained in KBr disks.

3. Results and discussion

In this study, we attempt to identify the effects of the adsorbed dyes on the pore structure of MCM-41 and the potential of MCM-41 for the removal of basic dyes. We first examine the adsorption capacity of BG5 and BV10 onto MCM-41.

3.1. Adsorption capacity of BG5 and BV10 on MCM-41

Fig. 2 shows the measured isotherms for BG5 and BV10 on the MCM-41 samples. For comparison, BG5 and BV10 adsorption on the Ca–montmorillonite (Ca-Mont) (Wang et al., 2004a) and activated carbon (purchased from Merck) are also demonstrated. As presented in Fig. 2, the adsorption of BV10 on MCM-41 possesses the largest capacity among the examined adsorbents, indicating that MCM-41 may be an attractive adsorbent for the removal of basic dyes from wastewater. This result is contrast to the report of Ho et al. (2003), i.e., MCM-41 is a poor adsorbent for Methylene blue with adsorption capacity only 54 mg/g. On the other hand, the adsorption capacity sequence for BG5 and BV10 may be varied for different adsorbents. For the Ca-Mont and activated carbon, the adsorption capacity of BG5 is larger than that of BV10, which is inverse proportional to the molecular sizes of adsorbates. For MCM-41, however, the adsorption capacity of BV10 is significantly higher than that of BG5, as manifested by the approximately 14-fold higher adsorption capacity of the BV10 (500 mg/g vs 36 mg/g). It is noteworthy that the adsorption capacity of BG5 on MCM-41 is similar to that of Methylene blue measured by Ho et al. (2003).

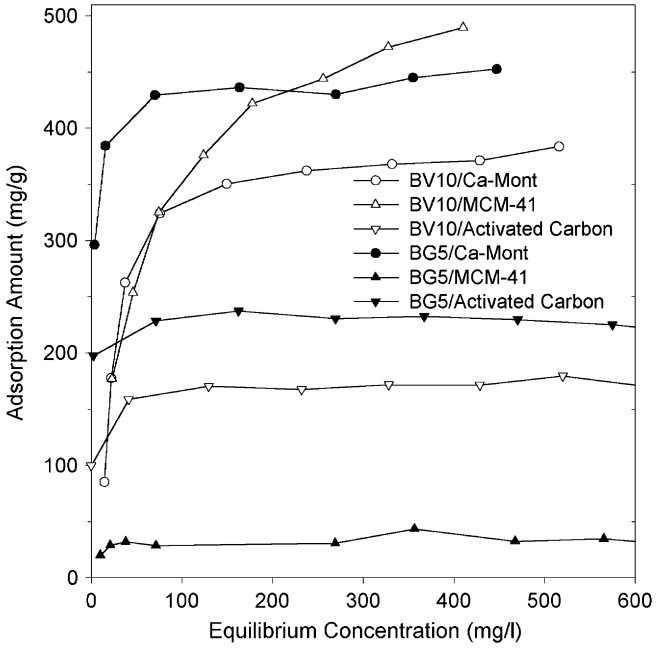

Fig. 2. Adsorption isotherms of BG5 and BV10 on MCM-41, activated carbon, and Ca–Mont at 25 °C and pH 4.

It is well known that the adsorption of basic dyes on montmorillonites is dominated by ion exchange processes (Wang et al., 2004a). The small difference in adsorption properties of Ca-Mont for BG5 and BV10 may be due to the capability of interlamellar expansion of montmorillonite and larger organic cations often act as "pillars" which keep the aluminosilicate sheets permanently apart (Dentel et al., 1998; Lee et al., 1999; Koh and Dixon, 2001). However, the significant difference existing in adsorption capacity for BG5 and BV10 on MCM-41 cannot be explained with the above adsorption mechanism because the intrinsically neutral characteristics of MCM-41 surface and the incapability of expansion of the cylindrical pore of MCM-41. Another way to interpret the above results may be with the aid of the difference existing in the interactions between basic dyes and surface hydroxyl groups of MCM-41. In general, it was found that the interactions between the incorporated dye molecules and MCM-41 were very strong (Stefan and Markus, 1999; Lia et al., 2006). On the other hand, it has been well established that the adsorbed Methylene blue on hydroxylated surface (e.g., MCM-41) is usually coordinated to four surface hydroxyl groups (Kaewprasit et al., 1998). Because the molecular configurations of both BG5 and BV10 are similar to the Methylene blue, the interaction configuration proposed above may be also applied to the systems of BG5 and BV10 on MCM-41. Accordingly, because the BG5 possesses more polar atoms (N and S), the interaction between BG5 and MCM-41 may be stronger than that between BV10 and MCM-41. This may induce a collapse in the pore structure of MCM-41, and then create a sharp decrease in the adsorption capacity. In follows, the revolutions of surface and pore structure of MCM-41 before and after adsorbing basic dyes are examined with the analysis of nitrogen isotherms, XRD patterns, and FTIR spectra to give some supports on the above deduction.

3.2. Effects of dye adsorption on the surface characteristics and pore structure of MCM-41

Fig. 3(a) shows the nitrogen adsorption–desorption isotherms measured on the MCM-41s before and after adsorbing BG5 and BV10. Some key features may be found directly from this figure. It can be seen that the monolayer capacity, thus the BET surface area of MCM-41, becomes smaller when basic dyes are adsorbed. This result implies that the large basic dyes may screen some MCM-41 surface rugosity, which becomes inaccessible for the nitrogen molecule and then, decreases the BET surface area. To examine whether or not the surface screening effect exists, we estimated and compared the surface fractal dimension D of all examined MCM-41s through the nitrogen isotherms with the aid of fractal version of Frenkel–Halsey–Hill equations. Usually, the obtained surface fractal dimension is between 2 and 3. A surface with $D = 2$ indicates that it is regular and smooth. A higher D value suggests a greater wiggle and space-filling surface. At a D value close to 3, the surface is extremely irregular. Therefore, the D value can be considered an operative measure of the surface roughness (Lee and Tsay, 1998). The classical Frenkel–Halsey–Hill theory on multilayer adsorption was extended to fractal surfaces

$$N/N_m \sim [RT \ln(P_0/P)]^{-1/m}, \quad (1)$$

where N/N_m represents the surface fractional coverage, and P and P_0 were the equilibrium and saturation pressures of the adsorbate, respectively. Two types of fractal isotherm equations were thus proposed (Lee, 2001). If the van der Waals attractions between the solid and adsorbed film is the dominating factor, then for self-similar surfaces,

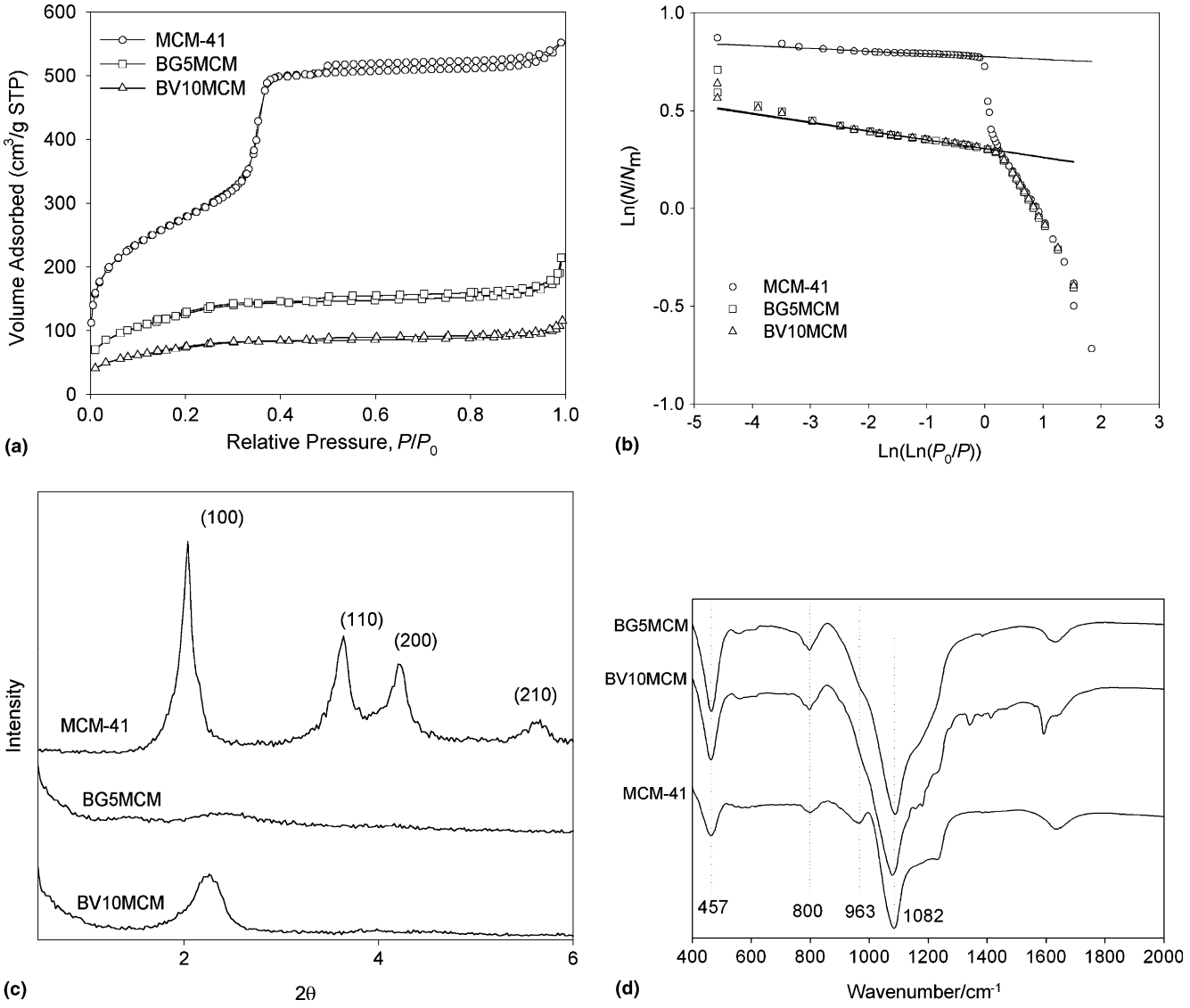

Fig. 3. (a) Nitrogen adsorption isotherms of the examined MCM-41s. The adsorption amounts for BG5MCM and BV10MCM are 32.5 and 376.2 mg/g, respectively. (b) Log–log plot of N/N_m vs $\ln P_0/P$ showing the linear range, where fractal behavior is observed. (c) XRD patterns of the examined MCM-41s. (d) FTIR spectra of the examined MCM-41s.

$$D = 3\left[1 - \frac{1}{m}\right]. \quad (2)$$

On the other hand, if the liquid/gas surface tension (capillary force) is more important, then for self-similar surfaces,

$$D = 3 - \frac{1}{m}. \quad (3)$$

The evaluation of D from Eqs. (2) and (3) for nitrogen isotherms on all examined MCM-41s is illustrated in Fig. 3(b) and the results are presented in Table 1. Because all samples show obvious capillary condensation in the mesopore range, we should use Eq. (3) to evaluate D. As demonstrated in Table 1, the changes of D values of MCM-41 during the adsorption processes of BG5 and BV10 are slight, indicating the surface screening effect is insignificant. Moreover, it is found that the D values for all MCM-41s are high (close to 3). For MCM-41, although its cylindrical pore structure is assumed to be high degree of pore symmetry, in some cases it still has opportunity to possess some larger and discontinuous inter-connected pores (Beck et al., 1992), which may induce the hysteresis loop in the nitrogen isotherm, as indicated in Fig. 3(a). The existence of these additional inter-connected pores may destroy the ideally shaped pore structures of MCM-41, and then increase the D values.

Another possibility for the reduction of the BET surface area induced by dye adsorption may come from the pore blocking effect, i.e., the large dye molecule may clog some smaller pores and inhibit the passage of nitrogen molecules into these pores. Because the surface screening effect is insignificant, the pore blocking effect may be responsible for the decrease of surface area induced by the dyes adsorption. This may be further revealed with the decrease in microporous area in MCM-41 after adsorbing BG5 and BV10, as shown in Table 1.

The other key feature in Fig. 3(a) is that primary MCM-41 shows clear capillary condensation at moderate nitrogen pressure. However, the capillary condensation phenomenon becomes diffuse when BG5 and BV10 are adsorbed on MCM-41, signifying the adsorption process may decrease the pore sizes uniformity. The pore sizes can be calculated from the X-ray diffraction interplanar spacing (Fig. 3(c)) and nitrogen isotherms (Fig. 3(a)) using the equation

$$S = bd(\rho V_p/(1 + \rho V_p))^{1/2}, \quad (4)$$

where S is the pore size, b is a constant dependent on the assumed pore geometry and is equal to 1.155 for hexagonal models, d is the XRD (100) interplanar spacing, V_p is the mesoporous volume, and ρ is the pore wall density (ca. 2.2 cm^3/g for siliceous materials) (Kruk et al., 1997). It is noteworthy that the average pore size of BG5MCM is difficult to estimate because the (100) peak is nonexistent in Fig. 3(c). As listed in Table 1, the adsorption of BV10 may decrease the pore size of MCM-41 to some extent.

Finally, the saturation adsorption capacity shown in Fig. 3(a) also suggests an enormous decrease in the total pore volume of MCM-41 after both BG5 and BV10 are adsorbed (see also Table 1). Obviously, the adsorption process of basic dyes leads to the simultaneous decrease in the specific surface area, pore size, and pore volume of MCM-41.

The XRD patterns accompanied with the adsorption processes are demonstrated in Fig. 3(c). The presence of both (100) and (200) diffraction peaks in the primary MCM-41 are evidence of good crystallinity of the prepared powder. However, a severe modification of the phase structure emerges from Fig. 3(c) after adsorbing BG5 and BV10. If the diffraction patterns are compared, it is clearly observed that BG5MCM is less crystalline than BV10MCM, indicated by the sharp decrease in the intensity of most MCM-41 peaks. Infrared spectra of MCM-41, BG5MCM, and BV10MCM were demonstrated in Fig. 3(d). As shown in Fig. 3(d), the three well-known vibrational modes of a-SiO_2 are visible in all spectra. These are the rocking mode near 457 cm^{-1}, the symmetrical stretching mode near 800 cm^{-1}, and the asymmetric stretching mode near 1082 cm^{-1} in which the oxygen atom vibrates along a line parallel to a line joining the adjacent silicon atoms. However, the absorption peak around 963 cm^{-1} observed in the MCM-41 disappears for both BG5MCM and BV10MCM, indicating the possibility of the collapse of the MCM-41 mesoporous structure (Gu et al., 1999). For BG5MCM, this collapse is further confirmed with the disappearance of (100) peak's signal of XRD patterns of MCM-41 shown in Fig. 3(c). However, the change in the pore structure of BV10MCM is more likely due to the inherent disorder induced by the adsorption of BV10 because the main peak signal of XRD pattern of MCM-41 still exists.

According to the adsorption capacity and the analysis of nitrogen isotherms, XRD patterns, and FTIR spectra, it is experimentally demonstrated that if the inherent disorder (in the pore structure of MCM-41) induced by basic dyes

Table 1
Specific surface areas, specific pore volumes, average pore diameters, and surface fractal dimensions for the examined samples

Solid	Abbreviation	BET surface area (m^2/g)	Micropore surface area (m^2/g)	Total pore volume (cm^3/g)	Micropore volume (cm^3/g)	Average pore diameter (nm)	Surface fractal dimension (D)
MCM-41	–	1003.5	39.9	0.76	0.01	3.96	2.99
BG5/MCM-41	BG5MCM	458.4	4.5	0.25	≈0	–	2.95
BV10/MCM-41	BV10MCM	265.8	4.9	0.13	≈0	2.11	2.96

is insignificant, MCM-41 may be a good adsorbent for the removal of basic dyes even no chemical modification on MCM-41 is taken.

In follows, the adsorption of BV10 onto MCM-41 with respect to pH, temperature, and contact time is discussed to provide more information about the effects of operation parameters on the basic dyes adsorption onto MCM-41.

3.3. The effect of pH on the adsorption of BV10

The pH value of the solution is an important controlling parameter in the adsorption process, as characterized in Fig. 4. It shows that the adsorption capacity of BV10 onto MCM-41 decreases significantly at low (2–3) and high (10–11) pHs. This result indicates that the higher or lower pH will not favor adsorption of the basic dye on MCM-41. Some other effects of pH on dyes and MCM-41 structure should be also considered. For instance, the dyes can be decomposed at acid solution and also the structure of MCM-41 may not be stable at acid solution.

3.4. Adsorption isotherms and dynamics of BV10 on MCM-41

BV10 adsorption isotherm data at different temperatures were measured and fitted into the model of Langmuir and Freundlich. The Langmuir equation is applicable to homogeneous adsorption system, while the Freundlich equation is an empirical equation employed to describe heterogeneous systems and is not restricted to the formation of the monolayer.

The well-known Langmuir equation is represented as

$$\frac{C_e}{Q_e} = \frac{1}{Q_{max}K_L} + \frac{C_e}{Q_{max}}, \tag{5}$$

where Q_e is the equilibrium BV10 concentration on the adsorbent (mg/g), C_e is the equilibrium BV10 concentration in solution (mg/l), Q_{max} is the monolayer capacity of MCM-41 (mg/g), and K_L is the Langmuir adsorption constant (l/mg). The Langmuir constant K_L is a measure of the affinity between adsorbate and adsorbent and its reciprocal value gives the concentration at which half the maximum adsorption capacity of the adsorbent is reached. A plot of C_e/Q_e vs C_e will give a straight line with slope $1/Q_{max}$ and intercept $1/Q_{max}K_L$ if Langmuir model is held (Özcan and Özcan, 2004). On the other hand, the Freundlich equation is represented as

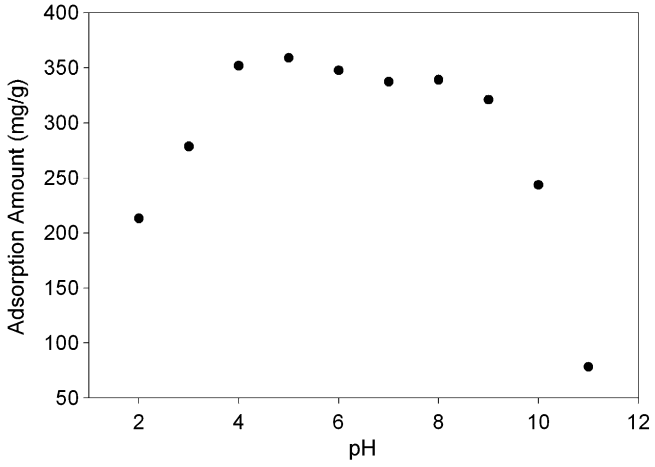

Fig. 4. Effect of pH on BV10 adsorption onto MCM-41 at 25 °C and initial concentration 500 mg/l.

$$Q_e = K_F C_e^{1/n}, \tag{6}$$

where K_F (l/g) and $1/n$ are the Freundlich constants corresponding to adsorption capacity and adsorption intensity, respectively (Özcan and Özcan, 2004). It is noteworthy that $1/n < 1$ (>1) corresponds to favorable adsorption (unfavorable adsorption) and to an increase (a decrease) in the adsorption capacity. The plot of $\ln Q_e$ vs $\ln C_e$ is employed to generate the intercept K_F and the slope $1/n$. In Fig. 5, both Langmuir and Freundlich model are fitted into the measured adsorption isotherms at different temperatures. The values of K_L, Q_{max}, K_F, $1/n$, and the linear regression correlations for Langmuir (r_L^2) and Freundlich (r_F^2) are given in Table 2. As listed in Table 2, the coefficients for fitting are $0.934 < r_L^2 < 0.999$ and $0.957 < r_F^2 < 0.978$ for Langmuir and Freundlich equation, respectively, indicating that Langmuir model should better describe the BV10 adsorption on the MCM-41, especially at lower adsorption temperatures. This seems to be consistent with the general accepted description of MCM-41, namely, the adsorption sites may be homogeneous distributed. The affinity parameter, K_L, varies from 2.89×10^{-3} to 1.91×10^{-2} l/mg and its reciprocal value varies from 346.02 to 52.36 mg/l. Both the affinity parameter and its reciprocal value indicate that the BV10 adsorption capacity on MCM-41 is largely perceptible to temperature changes. On the other hand, the values of $1/n$ are less than 1 at all temperatures, indicative of high adsorption intensity. If the values of K_F and $1/n$ are compared at all temperatures studied, it is found that higher values of $1/n$ and lower values of K_F are obtained at higher temperatures. These trends show that BV10 possesses higher adsorption capacity at lower temperatures.

The effect of contact time on the amount of BV10 adsorbed onto MCM-41 was measured at the optimum initial concentration and different temperatures. A simple kinetic analysis was performed with the aid of pseudo-second-order equation (Wang et al., 2004a,b). In this equation, the average value of the rate constant k can be calculated in the form

$$\frac{dQ_t}{dt} = k(Q_e - Q_t)^2, \tag{7}$$

where k is the rate constant, and Q_e and Q_t are the amount of dye adsorbed per unit mass of the adsorbent at equilibrium and time t, respectively. After definite integration by applying the initial conditions $Q_t = 0$ at $t = 0$ and $Q_t = Q_t$ at $t = t$, Eq. (7) becomes

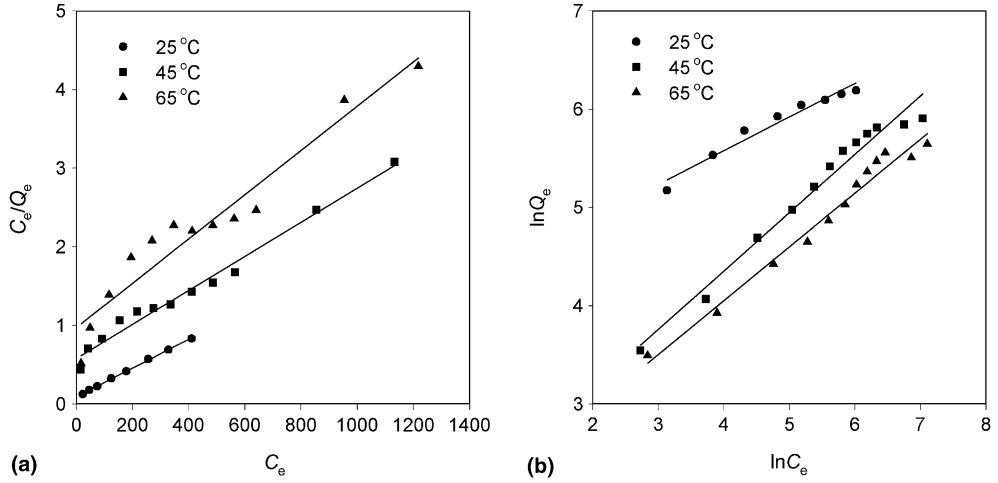

Fig. 5. Fitting (a) Langmuir and (b) Freundlich model to the adsorption isotherms of BV10 onto MCM-41 at pH 4 and different temperatures.

Table 2
Langmuir and Freundlich isotherm constants for the adsorption of BV10 on MCM-41

T (°C)	Langmuir			Freundlich		
	Q_{max} (mg/g)	K_L (l/mg)	r_L^2	$1/n$	K_F (l/g)	r_F^2
25	547.1	1.91×10^{-2}	0.999	0.34	67.5	0.957
45	462.2	3.70×10^{-3}	0.982	0.59	7.3	0.975
65	354.7	2.89×10^{-3}	0.934	0.59	6.6	0.978

$$\frac{t}{Q_t} = \frac{1}{kQ_e^2} + \frac{1}{Q_e}t. \tag{8}$$

The plot of t/Q_t vs t gives straight lines. Linear plots of the t/Q_t vs t in Fig. 6 with linear regression coefficients higher than 0.99 indicates the applicability of this kinetic equation and the pseudo-second nature of the adsorption process of BV10 onto MCM-41. The k values calculated from these plots are 6.70×10^{-4}, 2.59×10^{-3}, 1.66×10^{-2} g mg^{-1} min^{-1} for 25, 45, and 65 °C, respectively. Because the k values have been determined, several thermodynamic parameters including the Arrhenius activation energy (E_a), activation free energy change (ΔG^*), activation enthalpy change (ΔH^*), and activation entropy change (ΔS^*) can be calculated by using the following equations (Stumm and Morgan, 1996; Özcan and Özcan, 2004),

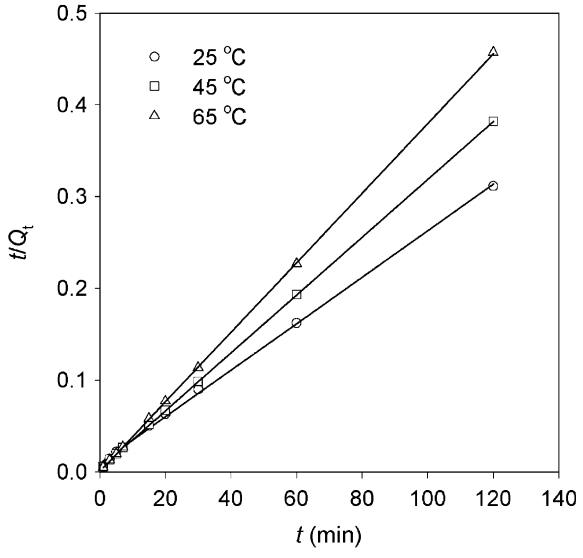

Fig. 6. The pseudo-second-order kinetics plots for the adsorption of BV10 on MCM-41. Conditions: initial dyes concentration 900 mg/l and pH 4.

$$\ln k = \ln A - \frac{E_a}{RT}, \tag{9}$$

$$k = \frac{k_B T}{h} K^*, \tag{10}$$

$$\Delta G^* = -RT \ln K^*, \tag{11}$$

$$\Delta H^* = E_a - RT, \tag{12}$$

$$\Delta S^* = \frac{\Delta H^* - \Delta G^*}{T}, \tag{13}$$

where A is the Arrhenius factor, k_B and h are Boltzmann's and Planck's constants, respectively, R is the gas constant, and K^* is the equilibrium constant at temperature T. A linear plot of $\ln k$ vs $1/T$ for the adsorption of BV10 onto MCM-41 is constructed to generate the E_a value from the slope. The result obtained is 66.9 kJ mol^{-1} with a linear regression coefficient 0.98. Moreover, the values of ΔG^*, ΔH^*, and ΔS^* are 84.1 (86.4, 86.7) kJ mol^{-1}, 64.4 (64.2, 64.1) kJ mol^{-1}, and −66.1 (−69.5, −67.0) J K^{-1} mol^{-1} at 25 (45, 65) °C, respectively. For comparison, these thermodynamic parameters are also estimated for BV10 adsorption on both Ca-Mont and activated carbon at conditions

of initial BV10 concentration 900 mg/l and pH 4. The values of ΔG^*, ΔH^*, and ΔS^* at 25 (45, 65) °C for BV10/Ca-Mont and BV10/activated carbon are 84.8 (90.1, 96.0) kJ mol^{-1}, 2.6 (2.5, 2.3) kJ mol^{-1}, and −275.9 (−275.7, −277.0) J K^{-1} mol^{-1} as well as 80.1 (86.1, 90.2) kJ mol^{-1}, 4.9 (4.7, 4.6) kJ mol^{-1}, and −252.4 (−256.0, −253.3) J K^{-1} mol^{-1}, respectively.

The slight high ΔH^* values for BV10/MCM-41 give a clear evidence that the interactions between BV10 and the surface hydroxyl groups of MCM-41 may be strong. On the other hand, the positive values of E_a, ΔG^*, and ΔH^* indicate the presence of an energy barrier in the adsorption process. The positive values for these parameters are quite common because the activated complex in the transition state is in an excited form. The negative values of ΔS^* suggest decreased randomness at the solid/solution interface and no significant changes occur in the internal structure of the adsorbent through the adsorption of BV10 onto MCM-41.

4. Conclusions

This study examined the possible effects of interaction between large dye molecules and MCM-41 on the pore structure of MCM-41 and the potential of MCM-41 for the removal of basic dyes. The adsorption capacity of BG5 and BV10 on MCM-41 was first measured and the changes in surface characteristics and pore structure of MCM-41 during the adsorption processes were then characterized with the analysis of the nitrogen isotherms, the XRD patterns, and the FTIR spectra. It was found that the adsorption capacity for the two dyes was very distinct although their molecular sizes were similar. The analysis of nitrogen isotherms indicated that dyes adsorption might result in a significant decrease in the specific surface area, pore volume, and pore size of MCM-41. Moreover, both the decrease in the (100) peak's signal of XRD patterns and the disappearance of absorption peak near 963 cm^{-1} in the FTIR spectra were observed for both dyes adsorption. For adsorbing BV10, the decrease in the crystallinity may be ascribed to the inherent disorder introduced by the adsorption process, but for adsorbing BG5, the decrease was more likely due to the collapse in the pore structure of MCM-41. It was concluded that although MCM-41 might be a good adsorbent for the removal of basic dye pollutants from effluents, the effects of the interaction between large dyes and surface hydroxyl groups of MCM-41 on the pore structure stability of MCM-41 must be considered because it might induce a sharp decrease in the adsorption capacity. With respect to the effects of pH, contact time, and temperature on BV10 adsorption onto MCM-41, it was found that the higher or lower pH will not favor BV10 adsorption onto MCM-41. Moreover, the Langmuir model was found to provide better description for the adsorption of BV10 on MCM-41 than the Freundlich model. On the other hand, the adsorption kinetics data could be well described with the pseudo-second-order kinetics model. The activation parameters could be evaluated with the pseudo-second-order rate constants. The slight high values of ΔH^* confirmed the strong interaction between large BV10 molecule and the surface hydroxyl groups of MCM-41.

Acknowledgements

The work was supported by Grants NSC92-2211-E-238-004 and NSC94-2211-E-238-001 of National Science Council (Taiwan, ROC).

References

Aronson, B.J., Blanford, C.F., Stein, A., 1997. Solution-phase grafting of titanium dioxide onto the pore surface of mesoporous silicates: synthesis and structural characterization. Chem. Mater. 9, 2842–2851.

Beck, J.S., Vartuli, C., Roth, W.J., Leonowicz, M.E., Kresge, C.T., Scmmitt, K.D., Chu, C.T.-W., Olson, D.H., Sheppard, E.W., McCullen, S.B., Higgins, J.B., Schlenker, J.L., 1992. A new family of mesoporous molecular sieves prepared with liquid crystal templates. J. Am. Chem. Soc. 114, 10834–10843.

Choma, J., Jaroniec, M., Burakiewicz-Mortka, W., Kloske, M., 2001. Critical appraisal of classical methods for determination of mesopore size distributions of MCM-41 materials. Appl. Surf. Sci. 196, 216–223.

Choudhary, V.R., Mantri, K., 2000. Temperature programmed desorption of toluene, *p*-xylene, mesitylene and naphthalene on mesoporous high silica MCM-41 for characterizing its surface properties and measuring heats of adsorption. Micropor. Mesopor. Mater. 40, 127–133.

Corma, A., 1997. From microporous to mesoporous molecular sieve materials and their use in catalysis. Chem. Rev. 97, 2373–2419.

Dentel, S.K., Jamrah, A.I., Sparks, D.L., 1998. Sorption and cosorption of 1,2,4-trichlorobenzene and tannic acid by organo-clays. Water Res. 32, 3689–3697.

Ghiaci, M., Abbaspur, A., Kia, R., Seyedeyn-Azad, F., 2004. Equilibrium isotherm studies for the sorption of benzene, toluene, and phenol onto organo-zeolites and as-synthesized MCM-41. Sep. Purif. Technol. 40, 217–229.

Gu, G., Ong, P.P., Chu, C., 1999. Thermal stability of mesoporous silica molecular sieve. J. Phys. Chem. Solids 60, 943–947.

Hansen, E.W., Courivaud, F., Karlsson, A., Kolboe, S., Stöcker, M., 1998. Effect of pore dimension and pore surface hydrophobicity on the diffusion of *n*-hexane confined in mesoporous MCM-41 probed by NMR-a preliminary investigation. Micropor. Mesopor. Mater. 22, 309–320.

Ho, K.Y., McKay, G., Yeung, K.L., 2003. Selective adsorbents from ordered mesoporous silica. Langmuir 19, 3019–3024.

Hu, X., Qiao, S., Zhao, X.S., Lu, G.Q., 2001. Adsorption of benzene in ink-bottle like MCM-41. Ind. Eng. Chem. Res. 40, 862–867.

Kaewprasit, C., Hequet, E., Abidi, N., Gourlot, J.P., 1998. Application of methylene blue adsorption to cotton fiber specific surface area measurement: part I. methodology. J. Cotton Sci. 2, 164–173.

Koh, S.M., Dixon, J.B., 2001. Preparation and application of organo-minerals as sorbents of phenol, benzene and toluene. Appl. Clay Sci. 18, 111–122.

Kruk, M., Jaroniec, M., Sayari, A., 1997. Structural and surface properties of siliceous and titanium-modified HMS molecular sieves. Mesopor. Mater. 9, 173–182.

Lee, C.K., 2001. Effect of heating on the surface roughness and pore connectivity of TiO_2: fractal and percolation analysis. J. Chem. Eng. Jpn. 34, 724–730.

Lee, C.K., Tsay, C.S., 1998. Surface fractal dimensions of alumina and aluminum borate from nitrogen isotherms. J. Phys. Chem. B 102, 4123–4130.

Lee, J.F., Lee, C.K., Juang, L.C., 1999. Size effects of exchange cation on the pore structure and surface fractality of montmorillonite. J. Colloid Interf. Sci. 217, 172–176.

Lee, J.W., Shim, W.G., Moon, H., 2004. Adsorption equilibrium and kinetics for capillary condensation of trichloroethylene on MCM-41 and MCM-48. Micropor. Mesopor. Mater. 73, 109–119.

Lia, D., Zhaoa, W., Suna, X., Zhanga, J., Anpob, M., Zhao, J., 2006. Photophysical properties of coumarin derivatives incorporated in MCM-41. Dyes Pigments 68, 33–37.

Liu, J., Feng, X., Fryxell, G.E., Wang, L.Q., Kim, A.Y., Gong, M., 1998. Hybrid mesoporous materials with functionalized monolayers. Adv. Mater. 10, 61–65.

Nooney, R.I., Kalyanaraman, M., Kennedy, G., Maginn, E.J., 2001. Heavy metal remediation using functionalized mesoporous silicas with controlled macrostructure. Langmuir 17, 528–533.

Oh, J.S., Shim, W.G., Lee, J.W., Kim, J.H., Moon, H., Seo, G., 2003. Adsorption equilibrium of water vapor on mesoporous materials. J. Chem. Eng. Data 48, 1458–1462.

Özcan, A.S., Özcan, A., 2004. Adsorption of acid dyes from aqueous solutions onto acid-activated bentonite. J. Colloid Interf. Sci. 276, 39–46.

Ribeiro Carrott, M.M.L., Candeias, A.J.E., Carrott, P.J.M., Ravikovitch, P.I., Neimark, A.V., Sequeira, A.D., 2001. Adsorption of nitrogen, neopentane, *n*-hexane, benzene, and methanol for the evaluation of pore sizes in silica grades of MCM-41. Micropor. Mesopor. Mater. 47, 323–337.

Selvam, P., Bhatia, S.K., Sonwane, C.G., 2001. Recent advances in processing and characterization of periodic mesoporous MCM-41 silicate molecular sieves. Ind. Eng. Chem. Res. 40, 3237–3261.

Stefan, E., Markus, S., 1999. Immobilization and catalytic properties of perfluorinated ruthenium phthalocyanine complexes in MCM-41-type molecular sieves. Micropor. Mesopor. Mater. 27, 355–363.

Storck, S., Bretinger, H., Maier, W.F., 1998. Characterization of micro- and mesoporous solids by physisorption methods and pore-size analysis. Appl. Catal. A: General 174, 137–146.

Stumm, W., Morgan, J.J., 1996. Aquatic Chemistry–Chemical Equilibrium and Rates in Natural Waters. Wiley, New Work.

Thomas, J.M., 1994. The chemistry of crystalline sponges. Nature 368, 289–290.

Wang, C.C., Juang, L.C., Hsu, T.C., Lee, C.K., Lee, J.F., Huang, F.C., 2004a. Adsorption of basic dyes onto montmorillonite. J. Colloid Interf. Sci. 273, 80–86.

Wang, C.C., Juang, L.C., Lee, C.K., Hsu, T.C., Lee, J.F., Chao, H.P., 2004b. Effects of exchanged surfactant cations on the pore structure and adsorption characteristics of montmorillonite. J. Colloid Interf. Sci. 280, 27–35.

Wloch, J., Rozwadowski, M., Lezanska, M., Erdmann, K., 2002. Analysis of the pore structure of the MCM-41 materials. Appl. Surf. Sci. 191, 368–374.

Ying, J.Y., Mehnert, C.P., Wong, M.S., 1999. Synthesis and applications of supramolecular-templated mesoporous materials. Angew. Chem. Int. Ed. 38, 56–77.

Zhao, X.S., Lu, G.Q., Hu, X., 2000. Characterization of the structural and surface properties of chemically modified MCM-41 material. Micropor. Mesopor. Mater. 41, 37–47.

Zhao, X.S., Lu, G.Q., Hu, X., 2001. Organophilicity of MCM-41 adsorbents studied by adsorption and temperature-programmed desorption. Colloid Surf. A: Physicochem. Eng. Aspects 179, 261–269.

Zhao, X.S., Lu, G.Q., Millar, G.J., 1996. Advances in mesoporous sieve MCM-41. Ind. Eng. Chem. Res. 35, 2075–2090.